Battery Charge Depletion Prediction on an Electric Aircraft

Quach Cuong Chi[1], Brian Bole[2], Edward Hogge[3], Sixto Vazquez[1], Matthew Daigle[4], José Celaya[5], Adam Weber[1], Kai Goebel[4]

[1] *NASA Langley Research Center, Hampton, VA 23681*
cquach@nasa.gov, sixto.l.vazquez@nasa.gov, adam.k.weber@nasa.gov

[2] *Department of Electrical and Computer Engineering, Georgia Institute of Technology, Atlanta, GA, 30332*
bbole3@gatech.edu

[3] *Northrop Grumman Technical Services , Hampton, VA 23681*
edward.f.hogge@nasa.gov

[4] *NASA Ames Research Center, Moffett Field, CA 94035*
matthew.j.daigle@nasa.gov, kai.goebel@nasa.gov

[5] *SGT, Inc., NASA Ames Research Center, Moffett Field, CA 94035*
jose.r.celaya@nasa.gov

ABSTRACT

Validation of prognostic technologies through ground and flight tests is an important step in maturing these novel technologies and deploying them on real-world systems. To this end, a series of flight tests have been conducted using an unmanned electric vehicle during which the motor system batteries were monitored by a prognostic algorithm. The research presented here endeavors to produce and validate a technology for predicting the remaining time until end-of-discharge of the batteries on an electric aircraft as a function of an expected future flight and online estimates of the charge contained in the batteries. Flight data and flight experiment results are presented along with an assessment of model and algorithm performance.

1. INTRODUCTION

Recent improvements in battery technology have increased energy density and capacity to the point of considering them for general aviation vehicles. Battery health management (BHM) is a safety-critical enabling technology for electric aviation. Safe adoption of battery-powered propulsion in aviation, however, suffers from difficulty in accurately estimating the total storage capacity in the batteries and determining the remaining useful capacity at any given instant during flight. This paper describes the application and assessment of a battery health prognostics system in an unmanned all-electric subscale aerial vehicle.

We develop a BHM system using a model-based framework on the Edge-540T electric aircraft (Saha et al., 2011). In model-based prognostics (Saha & Goebel, 2009; M. Orchard, Tobar, & Vachtsevanos, 2009; Daigle & Goebel, 2013; Luo, Pattipati, Qiao, & Chigusa, 2008), a model of the system under prognosis is developed for the purposes of state estimation and remaining life prediction. In this work, we compare the original particle filter-based implementation with a new unscented Kalman filter-based implementation that takes advantage of an improved battery model and new input prediction methods in order to improve health state estimation and end-of-discharge prediction performance.

This paper is organized as follows. Background information and motivation for the implementation of onboard battery health management algorithms for electric vehicles are given in Section 2. The prototype electric aircraft used to demonstrate battery charge estimation and battery end of discharge (EOD) prediction is described in Section 3. Battery state of charge (SOC) estimation and EOD prediction results are presented in Section 4 along with a description of relevant model-based filtering techniques. Uncertain EOD predictions made over a sample flight of the unmanned aerial vehicle (UAV) are presented and assessed in Section 5. Conclusions and future work are discussed in Section 6.

2. BACKGROUND

Electric propulsion has long been used in cars and small UAVs. Recently, improvements in battery storage capacity have made it possible for general aviation vehicle manufacturers to consider battery-powered solutions as well. With recent urgency to address environmental concerns, vehicle manufacturers are increasingly investing in electric alternatives (Harrup & Davis, 2010). Further, electric propulsion provides a number of operational and control advantages: reduced noise, no emissions, more responsive thrust, and reduced part count, to name a few. Use of battery-powered propulsion systems in manned and unmanned aircraft alike will require more sophisticated means of estimating available battery charge during operation. The estimation of remaining charge is not easily determined during usage and, in addition, each battery's charge storage capacity degrades over its life span.

As a result, operators of electrically-propelled aircraft are left making conservative estimates of mission time. And, if a significant change to the mission is required during flight, no simple method exists to determine actual versus required battery charge. In other words, an operator currently must have a reliable way to answer the following questions: 1) What is the required charge to complete the new mission?, and 2) What is the actual charge left in the batteries?

2.1. Battery Health Management Approaches

The main objective of BHM research is to create prognostic algorithms that provide accurate estimates of battery storage capacity during flight planning and accurate indication of remaining charge during flight. Battery system models for electric aircraft have been developed based on previous laboratory and field experiments by (Saha, Goebel, Poll, & Christophersen, 2009; Saha et al., 2011) and by (Daigle, Saxena, & Goebel, 2012). The work reported here covers testing and adapting the battery prognostic model to the flight environment of a real electric vehicle.

The applied approach is to develop and implement onboard BHM which monitors usage of the motor batteries and which runs estimation and prediction algorithms to: 1) determine the SOC, which expresses the remaining battery charge in a relative percentage; 2) predict the EOD, which is the total flying time; and 3) estimate the Remaining Useful Life (RUL), which is the remaining flying time from the present instant. The SOC is intended to be much like the fuel gauge in a conventional liquid fueled system. The RUL and EOD both describe similar information, which is to provide the operator some notion of how much operating time is remaining. The difference is that the EOD predicts the total flying time relative to the start of the flight, whereas the RUL predicts the remaining flying time relative to the current time. Because the charge storage capacity and other battery parameters are known to degrade over the battery's life, the underlying battery model must be tuned such that EOD predictions account for the life cycle degradation of the batteries.

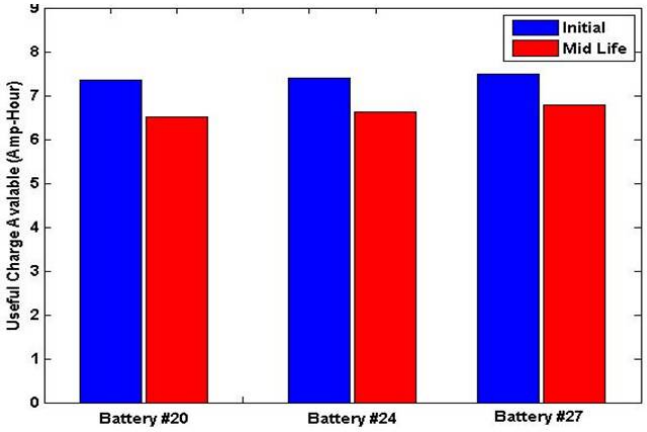

Figure 1. Useful charge available from new vs. old battery

2.2. Challenges in Online Computation of Battery SOC

In conventional liquid fuel systems, the remaining fuel level can be reliably measured and thus the remaining operating time can be obtained using vehicle and motor performance characteristics. This is because the volume of the tank is constant over the vehicle's lifespan. To the contrary, charge capacity in batteries can diminish over recharge cycles, and, depending on the chemistry used, over time as well. Part of the challenge of predicting the current battery SOC is determining the maximum capacity of constituent cells, which represents the initial condition of the discharge curve. As batteries age and experience an increasing number of recharge cycles, their maximum capacities diminish. Figure 1 illustrates this typical life cycle degradation for three batteries used in several flight experiments.

For this research, the charge capacity for a battery is the charge it can supply between its maximum rated voltage and the point when voltage drops precipitously under load. The precipitous drop is figuratively called the "knee point".

3. PROTOTYPE ELECTRIC VEHICLE DESCRIPTION

A 33% scaled Edge-540T, with electric propulsion, is used for this BHM research and development, as shown in Figure 2. It is 98 inches long with a 100 inch wing span and weighs 47.4 lbs., has 1881 in^2 of wing area with an average wing load of 0.025 psi.

The power system consists of two outrunner brushless DC electric motors mounted in tandem to drive a 26-inch propeller. The motor assembly turns the propeller up to 6000 RPM to develop about 37 pounds of thrust. Its airspeed ranges from a stall of 12 m/s to a dash of about 40 m/s (23-77

Figure 2. Picture of Edge-540T during landing

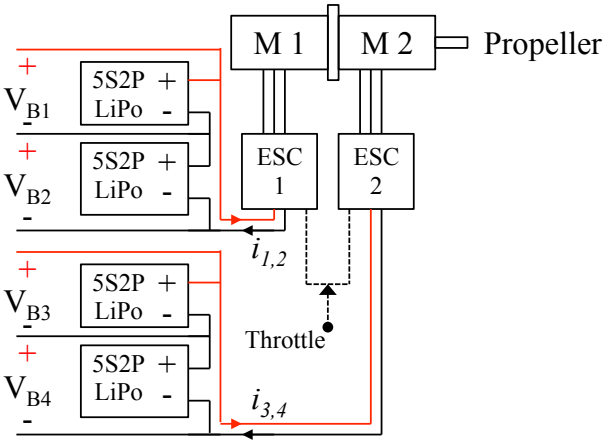

Figure 3. Motor System Diagram

Figure 4. Powertrain battery packs

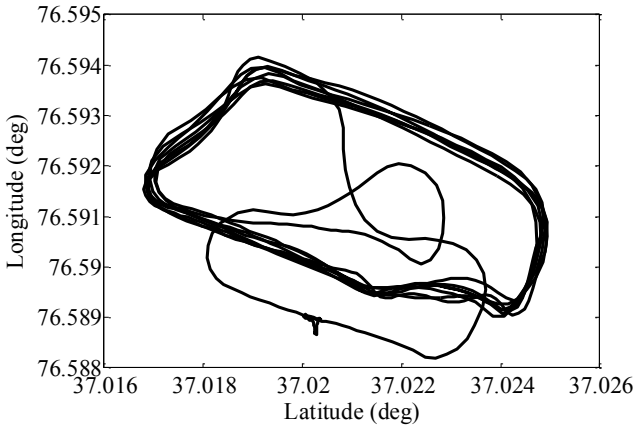

Figure 5. Ground track of flight

knots).

Electrical connections in the aircraft powertrain are illustrated in Figure 3. The two propeller motors are each powered by a series connection of two lithium-polymer (LiPo) battery packs. The power flow to the motors is controlled by a Jeti 90 Pro Opto electric speed controller (ESC). The ESC sends synchronized voltages to the motors at a duty cycle that is determined by a throttle input signal sent either by remote control from a pilot, or by an onboard autopilot.

Inductive loop current sensors are mounted on the positive lead feeding each ESC. Additional current sensors are also mounted on the positive feed from each of the four batteries. The positive lead of each battery is tapped to provide the data system with battery voltage measurements. These are the signals that the BHM system uses to estimate SOC, EOD, and RUL.

3.1. Energy Storage System

Each battery used to power the tandem motors consists of two sets of five series-connected 4.2 V 3900 mAh LiPo pouch cells, wired in parallel (Figure 4). The total rated capacity of each pack is 7800 mAh with a 50 C max burst discharge. The 50 C burst discharge allows a takeoff draw of up to 390 A. Takeoffs generally peak about 140 A. When fully charged, each 5-cell pack has an open circuit voltage of 21 V (4.2 V per cell). Two serially connected packs provide a maximum potential of 42 V to each motor.

The airplane is equipped with an autopilot that has the capability to navigate using a stored flight plan. A safety pilot typically flies the airplane from runway to test altitude and switches control to the autopilot, which proceeds to fly the flight plan. Figure 5 shows the ground track for a typical flight. Flight activities typically occur at 200 m above ground level. Flights last about 15 minutes with flight duration depending largely on throttle management.

A ground station interface monitors navigation and flight status using a vertical situation display, a moving map, and various text parameter displays. A second ground display monitors the powertrain batteries showing voltages, currents, remaining flight time, and state of charge for all four powertrain batteries.

3.2. Data System and Raw Data

The aircraft is instrumented with a real-time data system, described in (Hogge, Quach, & Hill, 2011). For the BHM research, the data system records battery voltage, current, and

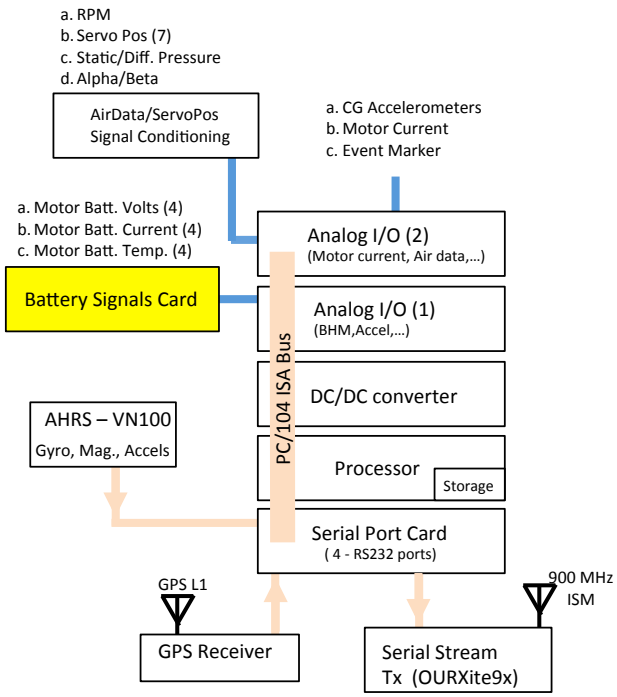

Figure 6. DAQ hardware diagram

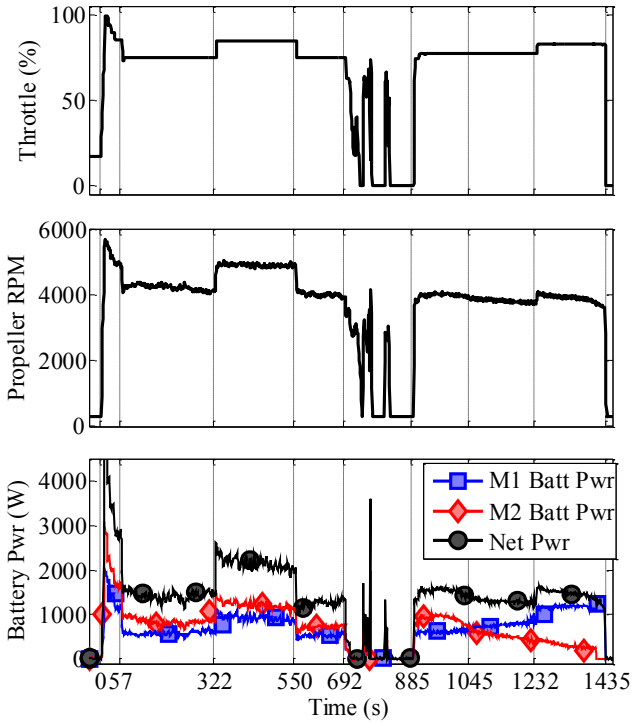

Figure 7. Plots of throttle command, propeller RPM, and battery power draw measured over a sample flight

temperature at 400 Hz. Figure 6 diagrams the data system hardware components. The data system also executes a battery prognostic model that computes the EOD, RUL, and SOC for all four batteries.

3.3. Flight Plan (Mission)

A sample flight of the Edge-540T electric aircraft is described in this section. This flight test includes: 1) a flight segment from take-off at 0 s to landing at 692 s; 2) taxiing to position from 692 s to 885 s; 3) operating the motor on the runway to discharge the batteries (885-1435 s). The experiment is stopped when the battery voltages drop below a specified cut-off threshold of 17 volts that designates the end of useful power delivery from the batteries.

The first flight segment (0-692 s) consists of essentially four activities. These include a take-off, followed by flight in auto-mode executing a flight plan at constant throttle set to 75%. The throttle is increased to 85% from 322 to 550 s. The throttle is then decreased to 75% from 550 to 692 s.

Figure 7 shows the throttle, propeller RPM, and battery power profiles recorded over a sample flight. Recall from Figure 3 that each motor is fed by a different circuit and that each circuit is powered by two batteries wired in series. The blue/square and red/diamond traces shown in Figure 7 give the net battery power input to the ESCs powering motors M1 and M2, respectively. The net battery power input to an ESC is given by the product of the current flowing through the ESC and the sum of the two series-connected battery voltages powering the ESC. The black trace in the battery power plot gives the sum of all battery power input to the two onboard ESCs.

Figure 8 shows the current and voltage profiles for three of the four batteries used to power the two propeller motors onboard the Edge-540T. The current and voltage data for battery B4 showed anomalous readings and are omitted from the plots in this paper. The ticks on the x-axis in Figures 7 and 8 denote the time of notable activities.

An interesting observation to note regarding the battery power draw over the sample flight is that motor M2 draws more power than motor M1 the majority of the time. This occurs until the batteries supplying power to motor M2 are depleted to about 18 volts each. At this point, the batteries powering motor M1 begin to take the majority load. This crossover is seen in both the battery power and battery current profiles at about the midpoint between 885 and 1232 s.

Relatively constant current draw is seen in Figure 8 for the three periods of constant throttle. Note the steep drop in voltage during the takeoff climb to below 20 V at time 0 and the subsequent voltage recovery by 57 s.

The period from 692 to 885 s in the figures shows the battery load when the pilot resumes control to land the airplane and get the airplane in position to operate the motors on the runway. Operating the motors on the runway to the end of

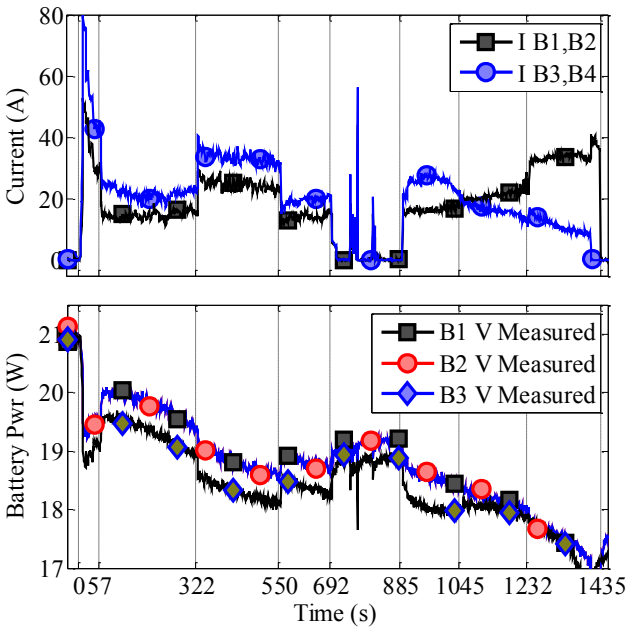

Figure 8. Battery current and Voltage profiles measured over sample flight

discharge for validation purposes, in lieu of flying until end of discharge, is more desirable as it abates the risk of a "dead stick" landing or a potential crash.

The period between 885 to 1435 s captures the ground discharge of the aircraft's batteries. This phase of the flight test is used to generate a ground truth measurement of the flight time that the batteries would have been able to support had the plane stayed in the air. For this segment, the pilot initially set the throttle to match the RPM range observed during the 75% constant throttle phase of the flight between 550 s and 692 s. For a constant throttle setting in the runway discharge, the propeller RPM, shown in Figure 7, trends downward and eventually drops below 4000 RPM. This is due to the weakened battery condition in the latter part of the discharge. Because the ground discharge is intended to imitate flight, the throttle was increased at time 1232 sec to raise the RPM above 4000 so as to meet output requirements for cruise flight.

The motors were stopped at 1435 s, after the batteries voltages were seen to fall below the 17 V threshold. Note that the net current draw is seen to increase as the net battery voltage decreases between 885 and 1232 s in order to meet the power demand dictated by the throttle set-point.

4. Battery Charge Depletion Prediction

Online battery prognostic algorithms are intended to estimate the present SOC and predict the EOD for the LiPo batteries that are used to power the aircraft's propeller motors. Separate battery systems are used to power the data acquisition and other flight communications and control hardware. The battery systems are sized such that it is always the case that the batteries powering the propeller motors will be the first to be depleted. For this reason, onboard battery discharge prognostic algorithms and supervisory decision making actions are only concerned with the propeller-driving batteries. Onboard battery charge depletion prediction routines will first estimate the current battery state, then these uncertain state estimates will be propagated into the future using uncertainty modeling of battery physics and uncertainty models for the future demands to be placed on the battery system.

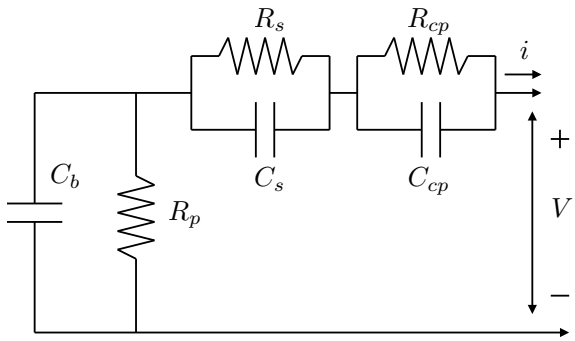

Figure 9. Equivalent circuit battery model

4.1. Battery Modeling

The current SOC of powertrain batteries is estimated using periodic battery current and voltage measurements along with a model that captures the current-voltage characteristics and how they vary as a function of battery charge (Pang, Farrell, Du, & Barth, 2001).

The model used here is an extended version of that presented in (Daigle et al., 2012). Figure 9 shows an equivalent circuit battery model that makes use of three resistor and three capacitor components that are each tuned to match the observed current-voltage dynamics of the batteries used to power the propeller motors on the Edge-540T. Battery charge is stored in the capacitor, C_b, in the equivalent circuit battery model. The R_s, C_s and R_{cp}, C_{cp} circuit element pairs capture battery internal resistance drops and concentration polarization effects, respectively. The resistor R_p is a large parasitic resistance that accounts for the slow battery self-discharge that is seen to occur over weeks or months of storage. Because battery current-voltage dynamics are known to vary as a function of battery SOC some of the resistive and capacitive (RC) components in the equivalent circuit model must be parametrized as functions of battery SOC (Zhang & Chow, 2010). It was decided based on qualitative observation that defining C_b, C_{cp}, and R_{cp} as parameterized functions of battery SOC gave an acceptable trade-off between the number of parameters to be identified and model error.

Table 1. Parameter values used in equivalent circuit model

Parameter	Value	Parameter	Value
q_{max}	2.88×10^4 C	C_s	89.3 F
C_{max}	2.85×10^4 C	R_{cp0}	1.60×10^{-3} Ω
C_{Cb0}	19.4 F	R_{cp1}	8.45
C_{Cb1}	1576 F	R_{cp2}	−61.9
C_{Cb2}	41.7 F	C_{cp0}	2689 F
C_{Cb3}	−203 F	C_{cp1}	$-2285\ F$
R_s	2.77×10^{-2}	C_{cp2}	−0.73 F

Battery SOC is defined as:

$$\text{SOC} = 1 - \frac{q_{max} - q_b}{C_{max}} \tag{1}$$

where q_b is the charge stored in the battery, q_{max} is the maximum charge that the battery can hold, and C_{max} is the maximum charge that can be drawn from the battery. The term coulombic efficiency is used to refer to the portion of stored charge that is recoverable during the discharge of the battery. There are some mechanisms including resting the battery that can unlock some of its lost capacity, however, the overall trend is inevitably downward.

C_b, C_{cp} and R_{cp} are parameterized as:

$$C_b = C_{Cb0} + C_{Cb1} \cdot \text{SOC} + C_{Cb2} \cdot \text{SOC}^2 + C_{Cb3} \cdot \text{SOC}^3 \tag{2}$$

$$C_{cp} = C_{cp0} + C_{cp1} \cdot \exp\left(C_{cp2}\left(\text{SOC}\right)\right) \tag{3}$$

$$R_{cp} = R_{cp0} + R_{cp1} \cdot \exp\left(R_{cp2}\left(\text{SOC}\right)\right) \tag{4}$$

where C_{Cb0}, C_{Cb1}, C_{Cb2}, C_{Cb3}, R_{cp0}, R_{cp1}, and R_{cp2} are empirical coefficients that are tuned based on observed current-voltage battery data over a range of SOC.

The current and voltage dynamics of the equivalent circuit model are defined as:

$$\mathbf{x}^B = \begin{bmatrix} q_b & q_{cp} & q_{Cs} \end{bmatrix}^T \tag{5}$$

$$\dot{\mathbf{x}}^B = \begin{bmatrix} -\frac{1}{C_b R_p} & \frac{1}{C_{cp} R_p} & \frac{1}{C_s R_p} \\ \frac{1}{C_b R_p} & -\frac{1}{C_{cp} R_p R_{cp}} & \frac{1}{C_s R_p} \\ \frac{1}{C_b R_p} & \frac{1}{C_{cp} R_p} & \frac{1}{C_s R_p} \end{bmatrix} \mathbf{x}^B + \begin{bmatrix} i \\ i \\ i \end{bmatrix} + \boldsymbol{\xi} \tag{6}$$

$$\mathbf{y}^B = V_p = \begin{bmatrix} \frac{1}{C_b} & \frac{1}{C_{cp}} & \frac{1}{C_s} \end{bmatrix} \cdot \mathbf{x}^B \tag{7}$$

where q_b, q_{cp}, and q_{cs} represent the charge stored in C_b, C_{cp}, and C_{cs} respectively, and the voltage drop across the battery terminals is equal to the sum of the voltage drops across each of the three capacitors.

The fitting of equivalent circuit RC parameters to the observed current-voltage response of the Edge-540T powertrain batteries is described in (Bole et al., 2013). The identified parameter values for the batteries used in the sample flight described in Section 3.3 are given in Table 1.

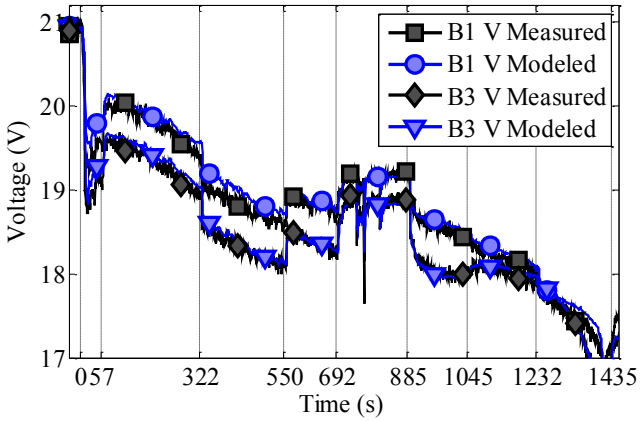

Figure 10. Modeled and measured voltages of batteries B1 and B3 for a sample flight loading profile

Figure 10 shows the predicted and measured voltage profiles for batteries B1 and B3 using the recorded battery current profiles shown in Figure 8. The close match between observed battery voltages and open-loop predictions made using the given loading profile provides a measure of validation for the fitted battery models.

4.2. Estimation

The identified battery model may be used to implement an observer for the internal battery states based on sampled voltage and current data. The unscented Kalman filter (UKF) (Julier & Uhlmann, 1997, 2004) and the particle filter (Arulampalam et al., 2002), are two flexible tools for preforming closed-loop updates of the probabilistic belief in system state estimates based on stochastic (and possibly nonlinear) models of system dynamics. Both approaches operate by drawing samples from probability distributions that are estimated for all of the uncertain parameters in the system state estimate and system dynamics model.

Particle filters use a discrete set of weighted samples, called *particles* to represent the belief in current system state estimates. Particles are sampled stochastically. The number of particles used and the methods used to assign weights and resample particles are design choices that will determine the computational overhead of this approach.

The UKF assumes a general nonlinear form of the state and output equations, and efficiently propagates model and state uncertainties without the need to calculate Jacobians (unlike the extended Kalman filter). The UKF is restricted to additive Gaussian noise random processes; however use of the unscented transform, a deterministic sampling method, allows random variables with non-Gaussian distributions to be incorporated using a minimal set of weighted samples, called *sigma points* (Julier & Uhlmann, 1997). The number of sigma points is only linear in the dimension of the random variable,

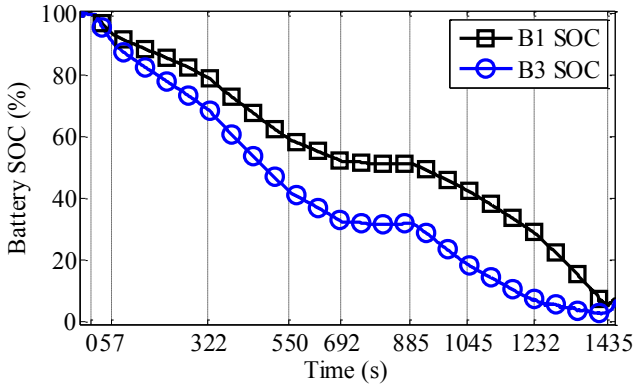

Figure 11. Estimated SOC for batteries B1 and B3 over flight

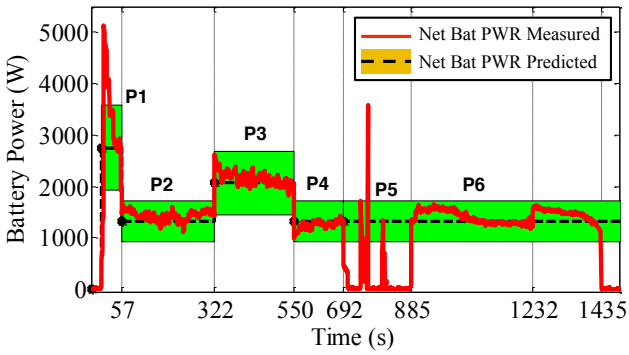

Figure 12. Measured and predicted net battery power consumption over sample flight. The six phases of the sample flight are annotated P1-P6

and so the statistics of the transformed random variable, i.e., mean and covariance, can be computed much more efficiently than by random sampling.

The use of a Kalman filter to update battery SOC estimates based on current and voltage samples is described in (Pang et al., 2001). The output of such closed-loop state estimation techniques will be much less susceptible to initialization and measurement errors than the Coulomb counting method currently used in many battery monitoring systems (Dai, Wei, & Sun, 2006).

Figure 11 shows the evolution of SOC estimates that are produced by a UKF algorithm acting on the voltage and current measurements for batteries B1 and B3 over the sample flight. The prior distribution of the process noise used in the UKF model is small here due to high confidence in the fitted battery model. The measurement noise is also assumed to be small due to accurate current and voltage sensing onboard the vehicle. The low measurement and process noise priors result in negligible uncertainty around SOC estimates in this case study. Therefore, uncertainty in the battery discharge prognostic estimates presented here is caused almost entirely by uncertainty in estimates of the future loads to be placed on system batteries.

4.3. Prediction

The batteries are considered to have reached the EOD condition when the battery voltage knee is observed under flight loads. The battery voltage knee is characterized by a precipitous drop in voltage that occurs at low battery SOC. The voltage knee is observed at approximately 1410 seconds for all of the powertrain battery voltages plotted in Figures 8 and 10.

In order to make a prediction, the future loading on the batteries and the corresponding uncertainty must be characterized in some fashion. In the sample flight described in Section 3.3, the aircraft flight plan is composed of the following phases;

1. takeoff and climb to $\sim$200 meters (duration = 60 s)
2. maintain altitude, set throttle to 75% (duration = 275 s)
3. maintain altitude, set throttle to 85% (duration = 228 s)
4. maintain altitude, set throttle to 75% (duration = 142 s)
5. land and taxi down the runway (duration = 193 s)
6. fully deplete batteries by spinning the propeller at similar RPMs those observed in phase 4.

The purpose of spinning the propeller at similar RPMs to that observed during 75% throttle flight is to safely obtain an approximate measurement for the amount of flight time that would have been supported by the battery pack if the aircraft had continued to be flown at the approximately the same speed as it was going in phase 4. This measurement allows comparison between battery EOD predictions made at various points over the sample mission, and the EOD time observed experimentally.

Subtracting the time spent landing and taxing on the runway (during which vary little power is drawn) from 1410 seconds, gives an approximate measurement for the time at which the EOD condition would have been observed if the aircraft had continued to be flown at the same speed as in phase 4 of the flight plan until EOD, $1410 - 193 = 1217$ seconds.

Figure 12 shows measured and predicted net battery power consumption over the sample flight. Future battery loading is estimated for the sample flight using knowledge of phases 1-4 in the flight plan enumerated above. The battery load predicted for phase 4 of the flight plan is assumed to continue until the battery system EOD condition is observed. The mean battery load prediction, shown as a dashed line in Figure 12, is estimated using a prior characterization of the energy required to perform aircraft maneuvers that are specified by a given flight plan. Characterization of net battery power required for the Edge-540T UAV to fly a given set of maneuvers is described in (Bole et al., 2013). A uniform probability distribution ranging $\pm 30\%$ from the mean battery load estimate

is added to future load estimates, denoted by the green band in Figure 12, to account for unmodeled system dynamics.

Given a state estimate, the prediction step proceeds by simulating that state estimate through time up until the EOD point, incorporating assumed future loading. For both the particle filter and UKF, the state estimate is represented by a set of weighted samples. The distribution of future loading, i.e., the battery power demand, is assumed to be constant over each leg of the flight. The constant demand over each leg of the flight is assumed to be drawn from a uniform distribution ranging $\pm 30\%$ from the mean battery load estimate. Here, we use the unscented transform to sample from the future loading distribution and obtain sigma points that cover the distribution, as described in (Daigle et al., 2012).

The equivalent circuit battery model is initialized for EOD prediction by taking a sample from the battery state estimate. The battery model is then simulated until EOD, using a battery load input that is drawn from the estimated distribution of possible future battery power demands. Just three sigma points are required to represent the uniformly distributed future battery loading demands. For a uniform distribution with the value used for the free parameter in the unscented transform yields the three points as the mean of the distribution and its two endpoints, thus naturally capturing the input bounds. The belief distribution for current system states is represented using nine samples from the UKF. The EOD belief estimate is then constructed by generating EOD estimates for all combinations of the nine samples representing battery state estimates, and the three samples of future battery load ($9 \cdot 3 = 27$ samples). This is much more efficient than when using the much greater number of samples from the particle filter.

5. Assessment

Figure 13 shows upper and lower bounds of RUL and EOD predictions for batteries B1 and B3, obtained using UKF for state estimation and the unscented transform for sample point identification. Although these projections are computed for all four batteries during the flight, only batteries B1 and B3 are shown in these graphs to avoid clutter. The figure shows the median, and range of the probability distribution calculated from the three simulated sigma points. RUL and EOD predictions are shown against the ground truth measurement of RUL and EOD obtained by fully discharging the batteries at flight loads on the ground. The ground truth measurements for EOD and RUL are shown as dashed lines in the figure. The ground truth RUL measurement is calculated by subtracting the current time from the EOD time, which was estimated to occur at 1217 seconds in Section 4.3 if the UAV had continued to fly at approximately the same speed as it was going in step 4 of the flight plan. An accuracy cone defined by $\alpha = 0.3$ is also shown for reference purposes. Predictions are shown at 60 s intervals. Here, we see that while the estimated RUL and EOD distributions seem to be converging to the true RUL and EOD as the flight progresses, there is a consistent over-estimation of EOD for battery B1 and a consistent under-estimation of EOD for battery B3 over the sample flight.

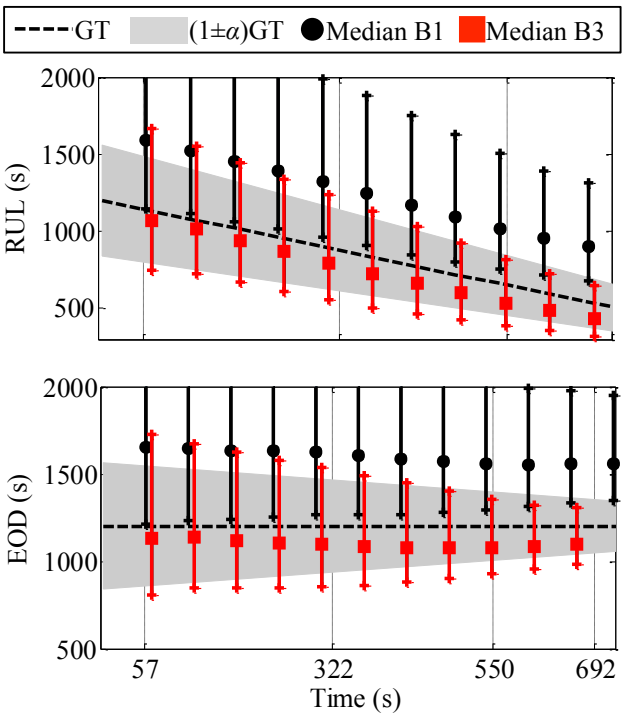

Figure 13. RUL and EOD predictions with future input trajectories drawn from a uniform distribution using the unscented transform.

The EOD estimation bias apparent in Figure 13 is explained by the fact that the battery demand modeling used assumes a constant split of power between the two tandem mounted propeller motors. However, as was shown in Figures 7 and 10, the power split between motors M1 and M2 is seen to change abruptly near the end of discharge.

Although the RUL estimates for B3 are seen to be slightly conservative, the estimates are fairly stable over the flight, and the estimated RUL probability density functions are seen to mostly fall within the 30% relative accuracy cone shown for the sample flight. This result is a considerable improvement on previous particle filter based implementations of battery EOD prognostics, that used the average of battery current over a finite window to estimate the future battery loading over a flight (Saha et al., 2011, 2009; Saha & Goebel, 2008; M. E. Orchard et al., 2012). Not only are the predictions more accurate, but they are more stable as well.

Figure 14 shows the mean RUL and EOD predictions obtained using a particle filter algorithm described in (Saha et

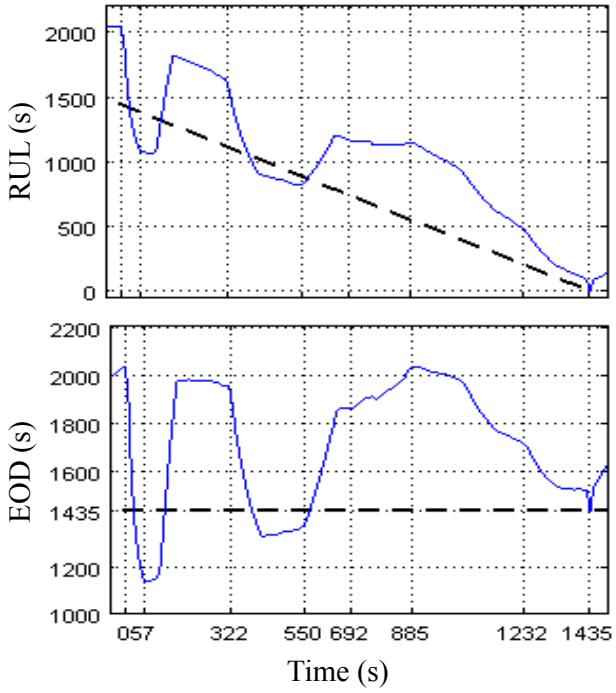

Figure 14. RUL and EOD predictions using particle filtering with future load estimated using a 100 second window of past current data

al., 2009), with a 100 s moving average used to project future battery current draw. Observe that the high current draw during takeoff does not reflect in reduced RUL until 57 s later; likewise, when the 75% constant throttle segment is started at the 57 s mark, the RUL does not stabilize until about 50 s later; and again at the 322 s throttle change. This effect is most pronounced on the throttle transition from the ground motor off to the ground discharge at 885 sec. This 50 s hysteresis could be reduced by reducing the width of the 100 s sliding window but at the expense of getting more jittery RUL projections which makes for a more unnerving operator experience. With a small window, the RUL predictions tend to fluctuate because when the load over the window is higher than what the load will be in the future, RUL is underpredicted, and when the load over the window is lower than the future load, RUL is overpredicted.

6. Conclusions

This paper described the application and assessment of battery charge depletion prognostics onboard an unmanned all-electric subscale vehicle. The paper also described a sample flight test during which a preplanned flight plan is autonomously flown by the aircraft. Predictions of available flight time remaining where generated based on measurements of the battery state of charge and knowledge of a flight plan. After a predetermined time the aircraft was landed and the propeller was spun at flight speeds to obtain a measurement of the actual flight time remaining. A unscented Kalman filtering based battery discharge prognostic algorithm was demonstrated, and the results were compared against a particle filtering based prognostic algorithm that had been published previously. Future work will involve additional flight tests, and improved input prediction methods that take advantage of known flight plans for improved accuracy.

Acknowledgment

The project support by NASA's AvSafe/SSAT and OCT/ACLO are respectfully acknowledged.

References

Arulampalam, M. S., Maskell, S., Gordon, N., & Clapp, T. (2002). A tutorial on particle filters for online nonlinear/non-Gaussian Bayesian tracking. *IEEE Transactions on Signal Processing*, *50*(2), 174–188.

Bole, B., Teubert, C., Chi, Q. C., Edward, H., Vazquez, S., Goebel, K., & Vachtsevanos, G. (2013). SIL/HIL replication of electric aircraft powertrain dynamics and inner-loop control for V&V of system health management routines. In *Annual conference of the prognostics and health management society.*

Dai, H., Wei, X., & Sun, Z. (2006). Online soc estimation of high-power Lithium-Ion batteries used on HEVs. In *IEEE international conference on vehicular electronics and safety.*

Daigle, M., & Goebel, K. (2013, May). Model-based prognostics with concurrent damage progression processes. *IEEE Transactions on Systems, Man, and Cybernetics: Systems*, *43*(4), 535-546.

Daigle, M., Saxena, A., & Goebel, K. (2012). An efficient deterministic approach to model-based prediction uncertainty. In *Annual conference of the prognostics and health management society.*

Harrup, P., & Davis, S. (2010). 21st century technology propels electric aircraft into the "blue yonder". *Power Electronics Technology*, *36*, 16-21.

Hogge, E. F., Quach, C. C., & Hill, B. L. (2011). *A data system for a rapid evaluation class of subscale aerial vehicle.* NASA/TM-2011-217145.

Julier, S. J., & Uhlmann, J. K. (1997). A new extension of the Kalman filter to nonlinear systems. In *Proceedings of the 11th international symposium on aerospace/defense sensing, simulation, and controls* (pp. 182–193).

Julier, S. J., & Uhlmann, J. K. (2004, March). Unscented filtering and nonlinear estimation. *Proceedings of the IEEE*, *92*(3), 401–422.

Luo, J., Pattipati, K. R., Qiao, L., & Chigusa, S. (2008, September). Model-based prognostic techniques applied to a suspension system. *IEEE Transactions on*

Systems, Man and Cybernetics, Part A: Systems and Humans, *38*(5), 1156 -1168.

Orchard, M., Tobar, F., & Vachtsevanos, G. (2009, December). Outer feedback correction loops in particle filtering-based prognostic algorithms: Statistical performance comparison. *Studies in Informatics and Control*, *18*(4), 295-304.

Orchard, M. E., Cerda, M. A., Olivares, B. E., & Silva, J. F. (2012). Sequential Monte Carlo methods for discharge time prognosis in Lithium-Ion batteries. *International Journal of Prognostics and Health Management*, *3*, 1-12.

Pang, S., Farrell, J., Du, J., & Barth, M. (2001). Battery state-of-charge estimation. In *American control conference.*

Saha, B., & Goebel, K. (2008). Uncertainty management for diagnostics and prognostics of batteries using Bayesian techniques. In *IEEE aerospace conference.*

Saha, B., & Goebel, K. (2009, September). Modeling Li-ion battery capacity depletion in a particle filtering framework. In *Proceedings of the annual conference of the prognostics and health management society 2009.*

Saha, B., Goebel, K., Poll, S., & Christophersen, J. (2009). Prognostics methods for battery health monitoring using a Bayesian framework. *IEEE Transactions on Instrumentation and Measurement*, *58*(2), 291-296.

Saha, B., Koshimoto, E., Quach, C. C., Hogge, E. F., Strom, T. H., Hill, B. L., ... Goebel, K. (2011). Battery health management system for electric UAVs. In *IEEE aerospace conference.*

Zhang, H., & Chow, M.-Y. (2010). Comprehensive dynamic battery modeling for PHEV applications. In *IEEE power and energy society general meeting.*

BIOGRAPHIES

Quach Cuong Chi got his M.S. from the School of Physics and Computer Sciences at Christopher Newport University in 1997. He is a staff researcher in the Safety Critical Avionics Systems Branch at NASA Langley Research Center. His research areas include development and testing of software for airframe diagnosis and strategic flight path conflict detection.

Brian M. Bole graduated from the FSU-FAMU School of Engineering in 2008 with a B.S. in Electrical and Computer Engineering and a B.S. in Applied Math. Brian received a M.S. degree in Electrical Engineering from the Georgia Institute of Technology in 2011, and he is currently pursuing a Ph.D. Brian's research interests include: analysis of stochastic processes, risk analysis, and optimization of stochastic systems. Brian is currently investigating the use of risk management and stochastic optimization techniques for optimal adaptation of active component load allocations in robotic and aviation applications. In a previous project, Brian worked with the Georgia Tech EcoCar team to develop an energy management controller for optimizing the fuel economy of a charge sustaining hybrid electric vehicle.

Edward Hogge received a B.S. in Physics from the College of William and Mary in 1977. He has provided engineering services to the government and currently is employed by Northrop Grumman Technical Services. He has recently been supporting aviation safety research through the implementation of electronic systems for subscale remotely piloted aircraft and through commercial aircraft simulation. He is a member of the American Institute of Aeronautics and Astronautics.

Sixto Vazquez Mr. Vazquez obtained MSEE from Old Dominion University in 1990 and BSEE from the University of Puerto Rico in 1983. He has developed real-time 3D graphical simulations to aid in the visualization and analysis of complex sensory data. Has developed techniques to interactively process, analyze, and integrate sensory data from multiple complex, state-of-the-art sensing technologies, i.e. FMCW Coherent Laser Radar range measuring system, Bragg grating Fiber Optic Strain Sensing system, etc., into simulation. In recent years, Mr. Vazquez has developed software for the ardupilot and associated ground station.

Matthew Daigle received the B.S. degree in Computer Science and Computer and Systems Engineering from Rensselaer Polytechnic Institute, Troy, NY, in 2004, and the M.S. and Ph.D. degrees in Computer Science from Vanderbilt University, Nashville, TN, in 2006 and 2008, respectively. From September 2004 to May 2008, he was a Graduate Research Assistant with the Institute for Software Integrated Systems and Department of Electrical Engineering and Computer Science, Vanderbilt University, Nashville, TN. From June 2008 to December 2011, he was an Associate Scientist with the University of California, Santa Cruz, at NASA Ames Research Center. Since January 2012, he has been with NASA Ames Research Center as a Research Computer Scientist. His current research interests include physics-based modeling, model-based diagnosis and prognosis, simulation, and hybrid systems.

Dr. José R. Celaya is a research scientist with SGT Inc. at the Prognostics Center of Excellence, NASA Ames Research Center. He received a Ph.D. degree in Decision Sciences and Engineering Systems in 2008, a M. E. degree in Operations Research and Statistics in 2008, a M. S. degree in Elec-

trical Engineering in 2003, all from Rensselaer Polytechnic Institute, Troy New York; and a B. S. in Cybernetics Engineering in 2001 from CETYS University, México.

Adam K. Weber is presently pursuing his B.S.E. in Aerospace Engineering at the University of Michigan, and is expected to graduate in December 2014. He is an intern in the Safety Critical Avionics Systems Branch at NASA Langley Research Center under the mentorship of Cuong Quach and Sixto Vazquez for a second year in a row. His research has included aiding in performance analysis and validation of a battery health management system and characterizing lithium polymer batteries.

Kai Goebel received the degree of Diplom-Ingenieur from the Technische Universitt Mnchen, Germany in 1990. He received the M.S. and Ph.D. from the University of California at Berkeley in 1993 and 1996, respectively. Dr. Goebel is a senior scientist at NASA Ames Research Center where he leads the Diagnostics & Prognostics groups in the Intelligent Systems division. In addition, he directs the Prognostics Center of Excellence and he is the Associate Principal Investigator for Prognostics of NASAs Integrated Vehicle Health Management Program. He worked at General Electrics Corporate Research Center in Niskayuna, NY from 1997 to 2006 as a senior research scientist. He has carried out applied research in the areas of artificial intelligence, soft computing, and information fusion. His research interest lies in advancing these techniques for real time monitoring, diagnostics, and prognostics. He holds eleven patents and has published more than 100 papers in the area of systems health management.